Cement and Concrete Research 40 (2010) 1114–1119

Contents lists available at ScienceDirect

Cement and Concrete Research

journal homepage: http://ees.elsevier.com/CEMCON/default.asp

Determination of elemental composition of cement powder by Spark Induced Breakdown Spectroscopy

N. Taefi, M. Khalaji, S.H. Tavassoli *

Laser and Plasma Research Institute, Shahid Beheshti University, G. C., 1983963113, Tehran, Iran

ARTICLE INFO

Article history:
Received 14 October 2008
Accepted 7 March 2010

Keywords:
Spark Induced Breakdown Spectroscopy
Cement powder
Spectroscopy (B)
Elemental analysis

ABSTRACT

Measurement of the cement powder composition as a major building material is considered very important. In this paper the capabilities of Spark Induced Breakdown Spectroscopy (SIBS) as a new technique for analysis of cement powder are shown. The major and minor elements of cement such as Ca, Si, Fe, K, Mg, Al, Na, Ba, Ti, V, Pb, Mn and Sr are detected qualitatively. For quantitative measurement, calibration curves are prepared for elements Ca, Si, Mg, Al, Fe and K with limit of detection below 220 ppm. The critical problems such as how to achieve quantitative measurement and improve the detection limits are investigated. The potential and drawbacks of SIBS technique in comparison with XRF for analysis of powder products are discussed.

1. Introduction

Powder materials represent the most common form of industrial raw materials. Industries like chemical, pharmaceutical, glass, ceramic, food, mining, metallurgy, construction and many others use the powder material in their application processes [1]. Determination of the elemental composition of these powder materials is critical in order to evaluate the product performance. Therefore much attention is presently devoted to continuous real-time measuring methods for analysis of these powder materials [2–5]. The measurement of cement elements is an important criterion for quality assurance of the cement powder. Cement is prepared by firing a mixture of raw materials in which Ca, Si, Al and Fe are their major elements. It also contains some minor elements such as Mg, Na, K and Ti. The cement chemical composition determines the quality and type of it. Minor elements can affect adversely the production and performance of cement. Because the level of these elements in the raw material varies from plant to plant, the required weight of lacking elements must be added to balance the cement composition [6–9]. This is possible by rigorous (permanent) testing of the final product, with online analysis methods. Consequently, the measurement of cement elements at the production line is an enforceable task.

In the present paper Spark Induced Breakdown Spectroscopy (SIBS) is introduced as an in situ method for analysis of cement powders and is compared with XRF. SIBS is an analytical technique for at-line concentration measurement of elements in some kind of samples. The basis of SIBS is monitoring of atomic emissions from hot plasma which is generated by a high voltage discharge between two electrodes. The plasma (spark) serves as both a method of sample introduction and an excitation reservoir. The plasma emission is collected by a fiber optics cable and transferred to a spectrograph equipped with an ICCD to record and analyze the data. The elements present in the sample are determined via their unique spectral lines.

The main advantages of SIBS which provide high potential for online measurement of materials are fast analysis method, absence of sample preparation and cheapness. Nowadays, analysis of cement powders are done with expensive and time consuming chemical methods, such as wet chemistry and XRF. Although XRF is the key technique for characterizing the elemental composition of material in cement factories, it needs sample preparation and expensive apparatus [10–12]. Furthermore, the detection limit of XRF changes with matrix type and it has poor sensitivity for lighter elements such as Cr and Ba [13,14]. Whereas the price of a typical XRF is more than 100,000$, the price of SIBS including high voltage sparker, spectrometer and analyzer software is about 40,000$ [12,15]. Table 1 shows potentials and weaknesses of SIBS in comparison with XRF. As it can be seen, there are some drawbacks for SIBS compared with XRF including lower sensitivity to heavy elements and higher

Table 1
Potentials and weaknesses of SIBS in comparison with XRF.

	SIBS	XRF
Sample preparation	No	Yes
Sensitivity to heavy elements	Low	High
Sensitivity to light elements	High	Low
Analyzing time	<10 s	>10 min
Relative error	<11%	<5%
Weight	<10 kg	>20 kg
Price	40,000$	100,000$

* Corresponding author. Tel.: +98 21 22431773; fax: +98 21 22431775.
E-mail address: h-tavassoli@sbu.ac.ir (S.H. Tavassoli).

0008-8846/$ – see front matter © 2010 Elsevier Ltd. All rights reserved.
doi:10.1016/j.cemconres.2010.03.003

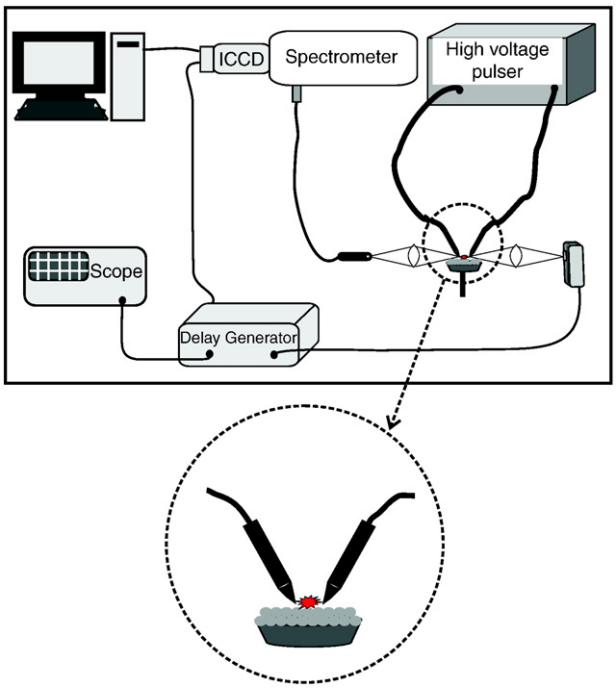

Fig. 1. Experimental set-up.

measurement error. So, the amount of further work is necessary to improve the weaknesses of SIBS and apply this technique with greater certainty.

SIBS is similar to Laser Induced Breakdown Spectroscopy (LIBS) in which a laser beam is focused onto a sample to generate the plasma [16–19]. SIBS is successfully used for analysis of metallic alloys [20] as well as monitoring heavy metals in airborne particulate materials [21,22]. In our knowledge, there are a few works using SIBS for powder samples. Hunter et al. used this method for rapid field screening of soils [14]. Their results include detection of Pb, Cr, Ba, Hg and Cd in soils and they indicate that SIBS can identify and quantitate a variety of environmentally interesting metals in soil matrices.

Here, the feasibility of using SIBS for the qualitative and quantitative analysis of elemental composition of loose powder samples is shown. Simultaneous qualitative detection of multiple elements (major, minor and trace elements) such as Ca, Si, Fe, K, Mg, Al, Na, Ba, Ti, V, Pb, Mn and Sr is done. The experimental parameters such as delay and gate times are adjusted to optimize the signal to background ratio. For quantitative determination of each element and preparation of calibration curve, several standard samples containing those elements are needed. In this work a series of national standard samples obtained from four different cement factories is used. Here, Ca, Si, Al, Fe as major and Mg, K as minor elements are presented in all samples and therefore, a calibration curve is prepared for each of them. The concentrations of calibrated elements in six samples are measured and compared with the results of XRF.

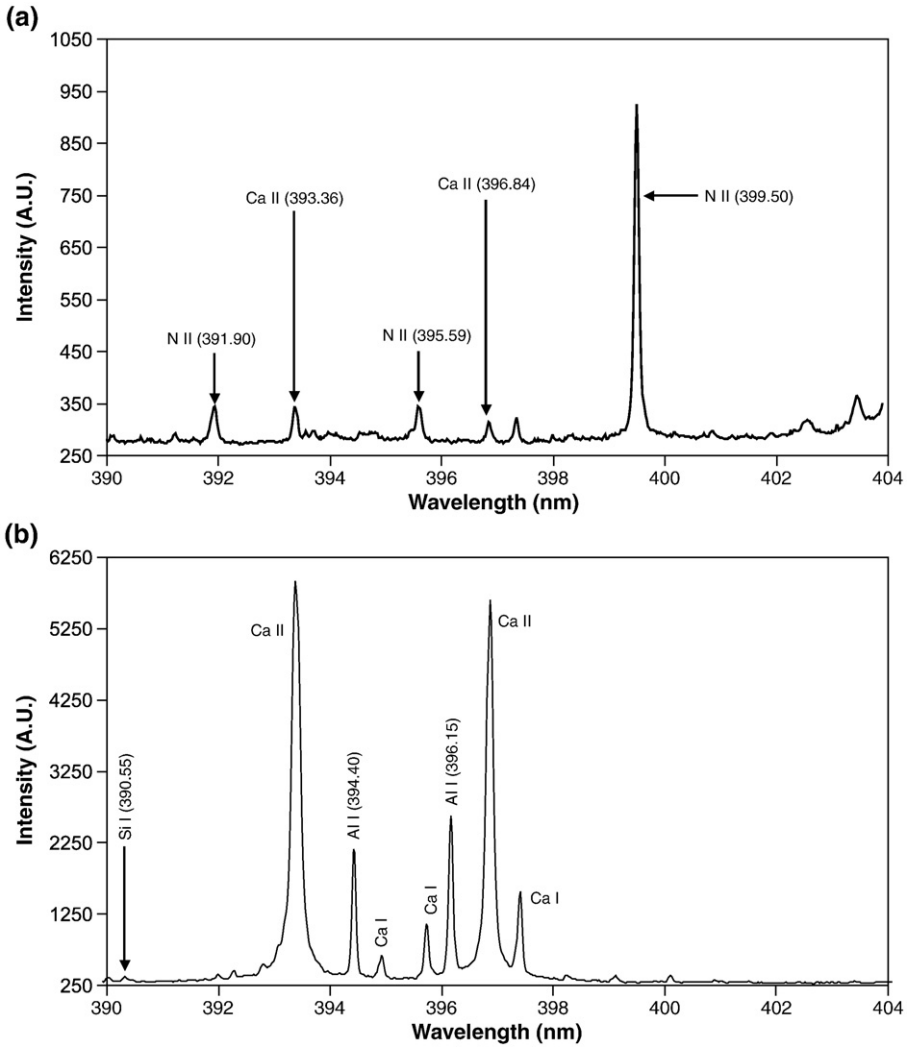

Fig. 2. SIBS spectrums of (a) air and (b) cement powder. Delay time 4.6 μs, gate width 10 μs.

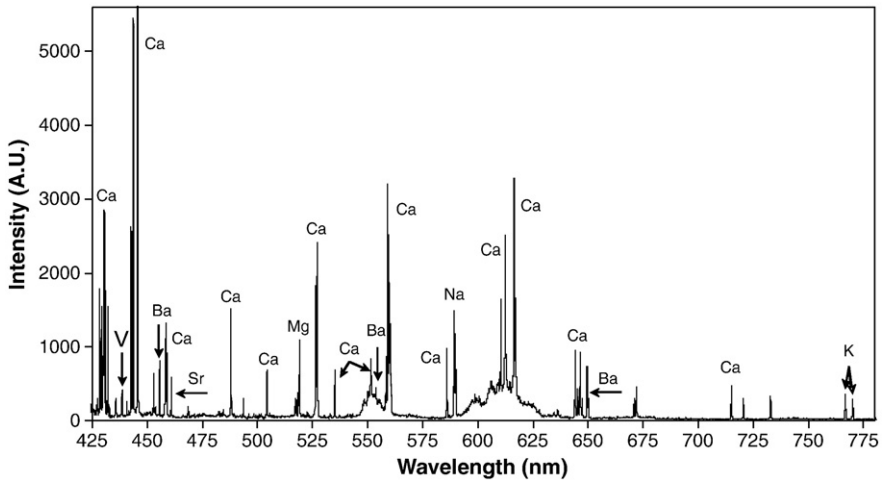

Fig. 3. A typical SIBS spectrum of major and minor elements. Delay time 50 μs, gate width 20 μs.

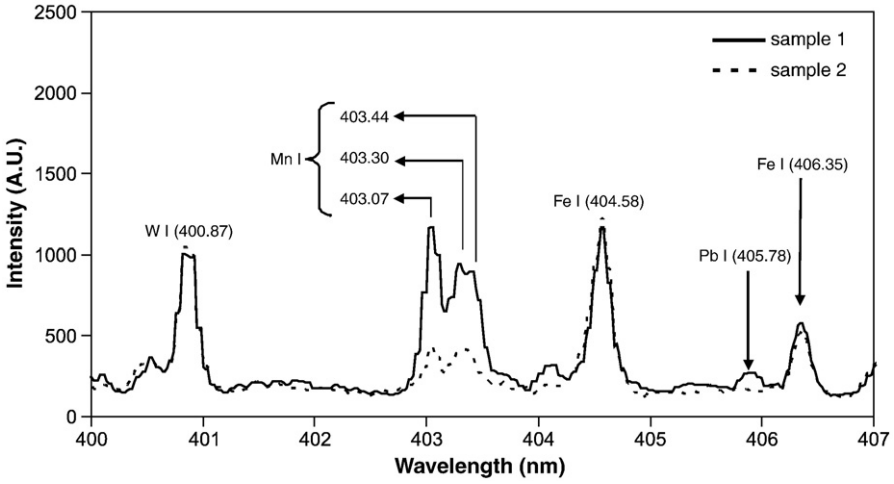

Fig. 4. SIBS spectrum of two different cement samples. Spectral lines of heavy metals are shown in this figure.

2. Experimental set-up

The experimental set-up used for the analysis of powder samples is shown in Fig. 1. This set-up includes a spark generating system and a detection system. The spark generating system is consisting of a high voltage power supply (12 kV, DC) integrated with a resistor–capacitor circuit (RC circuit). The spark energy is almost 2 J and has duration of 7.5 μs. The pulsed sparks occur between two 5 mm spaced tungsten electrodes placed close to the powder samples (2 mm). One of the electrodes is connected to the capacitors of the RC circuit and the other one is grounded. The charged capacitor discharges between electrodes by a triggerable switching spark gap that allows the spark to occur at set intervals. Consequently, air plasma is generated between electrodes. The resultant shock wave lifts some of the powder into the hot plasma region where any particle is vaporized and exited to emitting electronic states. As the plasma expands and cools gradually, the atomic and ionic emission lines appear. The emission from the plasma are focused on to a fast photodiode through a lens ($f = 5$ cm). A delay generator which is triggered by the photodiode signal is used to turns on the ICCD at an optimum delay time. At the other side, the plasma emission produced by spark collected by a lens ($f = 5$ cm) and transmitted by fiber optics to an Echelle spectrograph.

Table 2
Detected wavelength of each element and corresponding limit of detections (LOD).

Composition of cement samples (% W)						
Sample no.	CaO	Fe_2O_3	Al_2O_3	SiO_2	MgO	K_2O
1	62.09	2.89	3.36	19.33	3.02	0.91
2	58.39	3.24	4.61	25.26	2.75	0.45
3	49.38	3.09	4.46	35.78	2.67	0.66
4	57.27	3.49	6.81	24.46	1.31	0.52
5	63.60	3.70	4.96	21.24	2.85	0.68
6	56.89	3.68	6.25	26.56	2.47	0.85

Table 3
Composition of the cement samples measured by XRF.

Element	Wavelength (nm)	LOD (ppm)
Ca I	396.84	0.71
Mg I	517.26	4.5
Al I	396.15	4.7
Fe I	404.59	3.5
Si I	390.55	88
K I	766.49	220
Sr I	460.73	–
V I	440.82	–
Na I	588.99	–
Ba I	649.87	–
Pb I	405.78	–
Mn I	403.04	–
Ti I	453.20	–

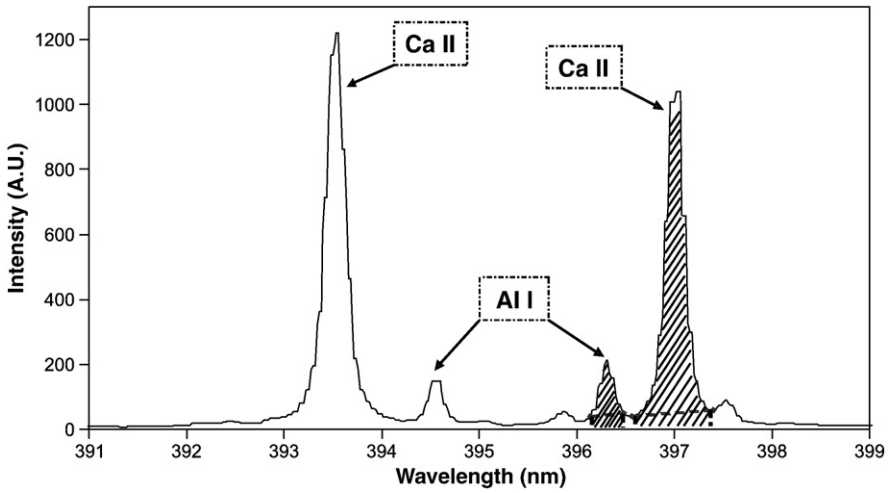

Fig. 5. Background subtraction by trapezoid method.

3. Results

The SIBS spectrums obtained from cement samples are used for qualitative and quantitative identification of them. The sample preparation is just consisted of pressing 5 g of cement powder into an insulated sample holder. As the amount of calcium oxide in cement is naturally high, the SIBS spectrum of cement samples are dominated by Ca I and Ca II emission lines. Fig. 2 shows the comparison between two SIBS spectrum recorded from air and a cement sample. Fig. 2(a) shows the strong spectral lines of N II in the spectrum of air plasma. As

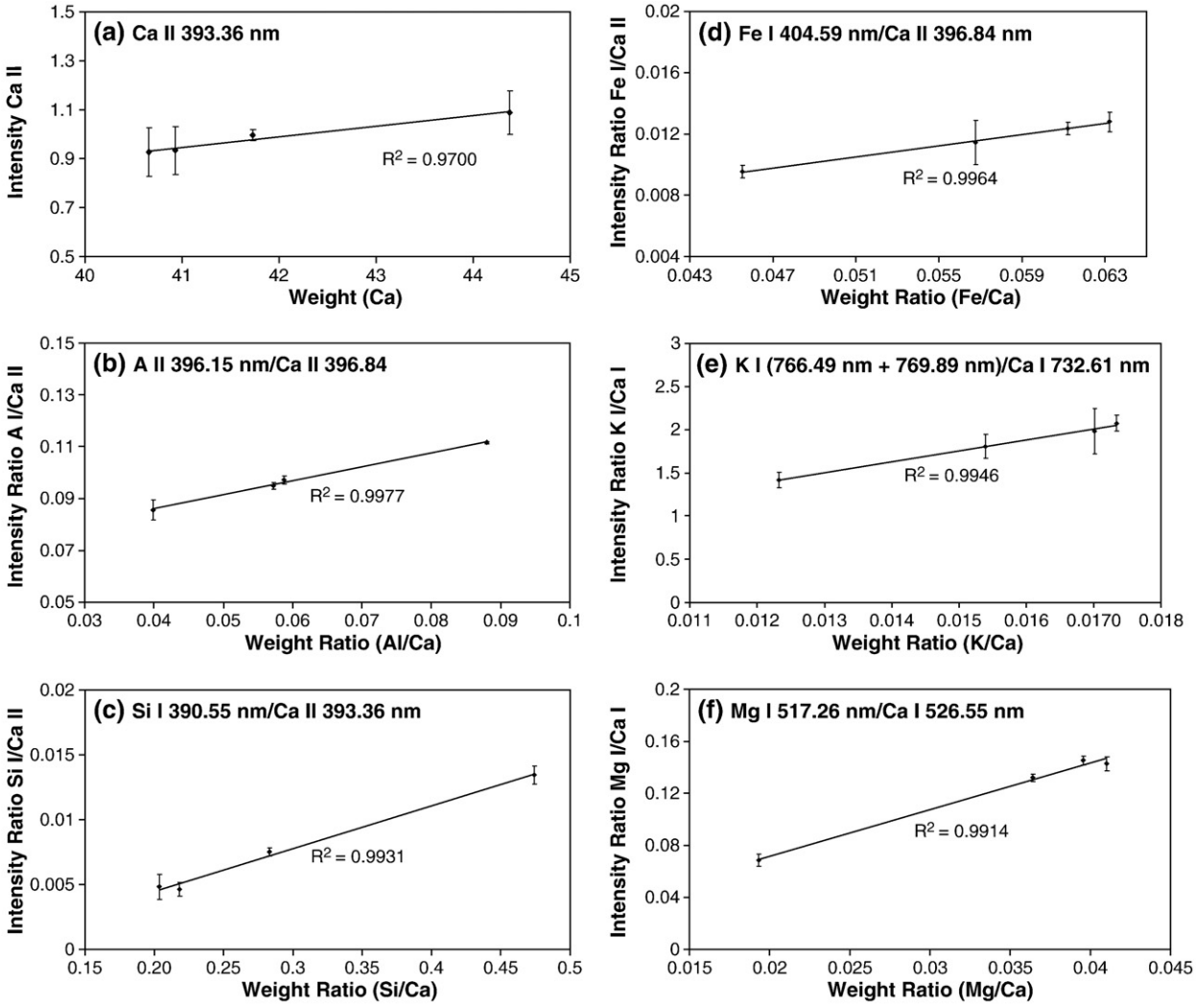

Fig. 6. Calibration curves for (a) Ca, (b) Al/Ca, (c) Si/Ca, (d) Fe/Ca (e) K/Ca and (f) Mg/Ca.

shown in this figure, the intensity of N II lines are much stronger compared with the intensity of Ca II lines. Fig. 2(b) shows a portion of SIBS spectrum for a cement sample at the same condition. The strongest Ca II lines are observed at 393.36 nm and 396.84 nm and the N II lines disappeared in this spectrum. In all experiments the spectral range 200–870 nm has been recorded simultaneously using an Echelle spectrometer. A portion of the spectrum from 425 to 775 nm is shown in Fig. 3. This part of spectrum shows narrow and intense atomic emission lines of Ca, Mg, Na, K and Sr elements. These lines are used to evaluate the concentrations of these elements. One of the advantages of SIBS over other direct analytical techniques (such as XRF) is the ability to detect lighter elements such as Ba [14]. As it can be seen in Fig. 3 this spectral window also contains the spectral lines of Ba I and Ba II. Because the amount of heavy metals in cement is important, we examine the presence of some heavy metals in cement samples. One of the heavy metals in cement is vanadium in which its spectral line at 440.82 nm is observed in Fig. 3. The spectral lines of other two heavy metals, lead (Pb) and manganese (Mn) for two kinds of sample are indicated in Fig. 4. This figure shows a spectral region from 400 to 407 nm. As it can be seen, although the amount of Fe for the two samples is approximately equal, the Pb and Mn lines are more intense in sample 1.

To evaluate the ability of this technique for quantitative analysis of powder samples, we prepared calibration curves for Ca, Fe, Al and Si as major and K and Mg as two minor elements. Preparation of calibration curves normally requires a series of appropriate certified samples. Here, six national standard samples of Portland cement collected from different cement factories are used as a multi-element standard of known composition. Four samples are used for preparing calibration curves and all samples are used as unknown samples for accuracy test. The elemental concentration of the samples is determined through analysis carried out by X-ray Florescence Spectroscopy. The concentrations of the analyzed constituents by XRF are given in Table 2. In our experiment operational parameters such as delay and gate times are adjusted to enhance the signal to background (S/B) ratio. This permits all major and minor elements to be measured at once. The S/B ratio also affects the sensitivity and measuring of the limits of detection (LOD) [23]. The optimized conditions are found at 50 μs delay time and 20 μs gate width. This long delay time is because the plasma is produced by a high pulse energy ($E_p = 2$ J). Two error sources in the experiment are variation in sampling volume in each spark event and fluctuation in the spark energy. For this reason, each measurement is the accumulation of 50 spark events and each data point represents the mean value of the three measured intensities on each sample. Another method which is wieldy used to correct or reduce the effect of these errors is based on internal standardization. In this method the intensity of elements is normalized to the intensity of a main component of the matrix [24]. Because the instabilities existing in spectral lines are almost the same, the normalization mainly eliminates the instabilities. Here, the main cement component, Ca, is taken as an internal standard. Since Ca is used as a normalization element, its concentration cannot be measured by the internal standard method. So, calcium is measured from calibration curve which is prepared using the absolute values.

For simultaneously analyzing of all elements of interest, the intense spectral lines which have minimal interference from other emission lines are chosen. The wavelengths of the identified elements are given in Table 3. The net peak area of each emission line is obtained in order to have the best linear correlation. Atomic emission lines are integrated and the background area subtracted by using the

Table 4
Comparison between XRF and SIBS measurements.

Sample #	CaO (%)	Ca (%)	Element	Normalized XRF	Normalized SIBS	W XRF (%)	W SIBS (%)	Absolute error (%)	Relative error (%)	Ave. abs. err.	Ave. rel. err.
1	62.09	44.3753	Al	0.040085887	0.039273782	1.778823529	1.742786139	0.036037391	2.025911522		
2	58.39	41.7309	Al	0.058483901	0.060710802	2.440588235	2.533518939	0.092930703	3.807717414		
3	49.38	35.2916	Al	0.066893424	0.070245153	2.361176471	2.479060674	0.117884203	4.992604519		
4	57.27	40.9305	Al	0.088083347	0.087857776	3.605294118	3.596061383	0.009232735	0.256088255		
5	63.6	45.4545	Al	0.057769478	0.056445309	2.625882353	2.565692941	0.060189412	2.2921595		
6	56.89	40.6589	Al	0.081380052	0.074139544	3.308823529	3.01443244	0.29439109	8.897152938	0.101777589	3.711939025
1	62.09	44.3753	Si	0.203590573	0.210551887	9.034394141	9.343304554	0.308910413	3.306222241		
2	58.39	41.7309	Si	0.28290612	0.292155519	11.80593875	12.19192489	0.385986144	3.269423572		
3	49.38	35.2916	Si	0.473845458	0.470725074	16.72274301	16.6126198	0.110123213	0.662888904		
4	57.27	40.9305	Si	0.279303734	0.314287264	11.43203728	12.86393017	1.431892883	11.13106854		
5	63.6	45.4545	SI	0.218396095	0.205106105	9.927083888	9.32299414	0.604089748	6.479568037		
6	56.89	40.6589	SI	0.305309001	0.369346618	12.41352863	15.01722777	2.603699141	20.97468995	0.907450257	7.637310206
1	62.09	44.3753	Mg	0.041036168	0.039820764	1.820992556	1.767058607	0.053933949	3.05218789		
2	58.39	41.7309	Mg	0.039735231	0.040516547	1.658188586	1.690793665	0.032605079	1.966307056		
3	49.38	35.2916	Mg	0.045618573	0.03242804	1.609950372	1.144435972	0.4655144	40.67631672		
4	57.27	40.9305	Mg	0.019298592	0.019303604	0.789900744	0.79010586	0.000205116	0.025960623		
5	63.6	45.4545	Mg	0.037806743	0.03660193	1.718486352	1.663722179	0.054764173	3.291665757		
6	56.89	40.6589	Mg	0.036630474	0.036868884	1.489354839	1.499048306	0.009693467	0.650850057	0.102786031	8.277214684
1	62.09	44.3753	Fe	0.045549263	0.04580237	2.021262525	2.032494217	0.011231692	0.552606336		
2	58.39	41.7309	Fe	0.054301485	0.050324414	2.266052104	2.100085173	0.165966931	7.324056271		
3	49.38	35.2916	Fe	0.061236811	0.061138161	2.161142285	2.157660754	0.003481531	0.161356757		
4	57.27	40.9305	Fe	0.059635301	0.056211706	2.440901804	2.300772373	0.140129431	6.090538657		
5	63.6	45.4545	Fe	0.056931127	0.056127642	2.587775551	2.551253522	0.036522029	1.431532715		
6	56.89	40.6589	Fe	0.063301946	0.063642637	2.573787575	2.587639715	0.01385214	0.538200593	0.061863959	2.683048555
1	62.09	44.3753	K	0.016199859	0.016033863	0.71887372	0.711507596	0.007366124	1.035283979		
2	58.39	41.7309	K	0.008518547	0.013484268	0.355487004	0.562711219	0.207224215	58.29304925		
3	49.38	35.2916	K	0.014773533	0.015847665	0.52138094	0.559288749	0.037907809	7.270654888		
4	57.27	40.9305	K	0.01486124	0.014756316	0.608277763	0.603983159	0.004294604	0.711047041		
5	63.6	45.4545	K	0.011817981	0.011884124	0.537180362	0.540186837	0.003006475	0.556561998		
6	56.89	40.6589	K	0.016514845	0.016719623	0.671475453	0.679801495	0.008326042	1.239962267	0.044687545	11.5177599
1	–	–	Ca	–	–	44.3753067	43.2244965	1.150810204	2.662402797		
2	–	–	Ca	–	–	41.73094151	42.04248128	0.31153977	0.741011853		
3	–	–	Ca	–	–	35.29155492	40.85382224	5.562267318	13.61504754		
4	–	–	Ca	–	–	40.93048502	41.23513481	0.304649784	0.738811176		
5	–	–	Ca	–	–	45.45449358	40.37164031	5.082853269	12.59015792		
6	–	–	Ca	–	–	40.65890157	41.15382091	0.494919337	1.202608473	2.15117328	5.258339959

trapezoid method. In this method an imaginary line between either two sides of the spectral line is considered, then the area under this line is subtracted as the background [23]. The emission signal is computed as the area above the imaginary line. This is shown in Fig. 5 with lines due to the elements Al and Ca. This method can be used for all emission lines especially in complex cases. The corresponding normalized calibration curves are given in Fig. 6. To achieve the highest value of correlation for each element a proper line of both analyte and standard element are selected. The proper emission lines have been chosen by comparing the resultant calibration curves of each element obtained by using different emission lines. The selected elemental wavelengths and their corresponding Ca lines are indicated in Fig. 6. The results show that reliable calibration curves are obtained for the lines which are as close as possible in wavelengths and upper energy levels. The highest correlation coefficient for K is achieved by using the sum of the intensities of two lines at 766.49 nm and 769.89 nm. The calibration curve for Fe is achieved using spectral line at 404.58 nm. The selected line is not the most intense one in comparison to other lines of this element, but the calibration coefficient is the highest for this line. This is because this line is free from spectral interference with the other elements. Calibration curves for the major elements are very reproducible and regression values, R^2 for analyte elements are close to unity. The error bars indicate the relative standard deviation, RSD. The RSD values are lower for the major elements in which their concentrations are more than about 20% by weight. Elemental analysis shows that the difference in RSD for elements can be due to the inhomogeneous distribution of the element across the samples [25]. LOD are calculated from the usual expression, LOD $= 3\frac{\sigma_B}{S}$ where σ_B is the standard deviation of the background emission and is the slope of the calibration curves. The calculated detection limits for Ca, Al, Fe, Si, K and Mg are given in Table 3. The results of this table show that this technique can be a reliable one for online analysis of powder products compared to the other methods such as XRF. Table 4 shows a comparison between XRF and SIBS measurements. In this table six national standard samples are used as unknown samples and their composition determined via prepared calibration curves. As it can be seen, the average absolute error for Ca, Al, Si, Mg, Fe and K is 2.15%, 0.10%, 0.91%, 0.10%, 0.06% and 0.05%, respectively. Also, the average relative error for Ca, Al, Si, Mg, Fe and K is 5.26%, 3.71%, 7.82%, 6.28%, 2.62%, and 11.52%, respectively. Absolute errors of calcium are higher compared with other elements because it has higher concentrations among the measured elements. Also, potassium has higher relative errors because it has lower concentrations among the other elements.

4. Conclusion

In this paper a complete qualitative elemental analysis of cement powder are achieved by Spark Induced Breakdown Spectroscopy. Major (Ca, Al, Fe, and Si) and minor elements (K, Na, Mg, Ba, Ti and Sr) and heavy metals (V, Mn, and Pb) are detected by this method. The results show that quantitative determination of major and minor elements of powder samples is possible with this technique. For quantitative analysis, internal standard method is used in which the emission intensities of each element are normalized to the emission intensity of a proper Ca atomic line. Use of area under the peak instead of peak values, together with the normalization to the continuum emission intensity improves the correlation coefficient in the calibration curves. For elements Ca, Si, Mg, Al, Fe and K calibration curves are prepared with linear regression coefficients between 0.970 and 0.997. The limits of detection below 220 ppm are found, although lower limits can be achieved by improving the spark generating and sampling systems. This study shows that by improving the weaknesses of SIBS it can be used as an economic system with useful application in industry for on line analysis of powder samples.

References

[1] J.P. Singh, S.N. Thakur, Laser-Induced Breakdown Spectroscopy, ELSEVIER, Chichester, 2007.
[2] P.O. Verkhovodov, Routine X-ray fluorescence analysis of powder materials using the "VERBA-XRF" mode, X-Ray Spectrom 33 (2004) 273–276.
[3] H. Shan, S. Zhuo, R. Shen, C. Sheng, Mineralogical effect correction in wavelength dispersive X-ray florescence analysis of pressed powder pellets, Spectrochimica Acta Part B: Atomic Spectroscopy 63 (2008) 612–616.
[4] J.F. Archambault, A. Vintilou, E. Kwong, The effects of physical parameters on laser-induced breakdown spectroscopy analysis of intact tablets, AAPS PharmSciTech 6 (2005) 253–261.
[5] F.S. Jerneja, S.S. Irena, G. Svegl, Proficiency testing of chloride content in different types of Portland cement, Accred. Qual. Assur. 11 (2006) 414–421.
[6] M.Y. Hassaan, Basalt rock as an alternative raw material in Portland cement manufacture, Mater. Lett. 50 (2001) 172–178.
[7] A. Monshi, M.K. Asgarani, Producing Portland cement from iron and steel slags and limestone, Cem. Concr. Res. 29 (1999) 1373–1377.
[8] F.B. Reig, V.P. Martinez, J.V.G. Adelantado, S.S. Ramos, D.J.Y. Marco, F.B. Mossi, X-ray fluorescence analysis of iron (III), potassium and sulfur oxides in cements with a hyperbolic addition–dilution model and using a single multicomponent standard, J. Anal. At. Spectrom. 13 (1998) 583–585.
[9] J.I. Bhatty, Effect of Minor Elements on Clinker and Cement Performance: A Laboratory Analysis Research and Development, Portland Cement Association, 2006 Bulletin RD130.
[10] M.K. Tiwari, A.K. Singh, K.J. Sawhney, Sample preparation for evaluation of detection limits in X-ray fluorescence spectrometry, Anal. Sci. 21 (2005) 143–147.
[11] M. Gaft, I. Sapir-Sofer, H. Modiano, R. Stana, Laser induced breakdown spectroscopy for bulk minerals online analyses, Spectrochimica Acta Part B 62 (2007) 1496–1503.
[12] Reinhard Noll, Holger Bette, Adriane Brysch, Marc Kraushaar, Ingo Monch, Laszlo Peter, Volker Sturm, Laser-induced breakdown spectrometry applications for production control and quality assurance in the steel industry, Spectrochimica Acta Part B 56 (2001) 637–649.
[13] Y. Kim, T. Yang, M. Lee, K. Lee, Quantitative analysis of pottery glaze by laser induced breakdown spectroscopy, Micro chem. J. 68 (2) (2001) 251–256.
[14] A.J.R. Hunter, R.T. Wainner, L.G. Piper, S.J. Davis, Rapid field screening of soils for heavy metals with spark-induced breakdown spectroscopy, Appl. Optics 42 (12) (2003) 2102–2109.
[15] http://www.bruker-axs.de/uploads/tx_linkselectorforpdfpool/ASTM-Cement-C-114-Qualification_05.pdf.
[16] A.W. Miziolek, V. Palleschi, I. Schechter, Laser Induced Breakdown Spectroscopy, Fundamentals and Applications, Cambridge University Press, 2006.
[17] R.S. Harmon, F.C. De Lucia, A.W. Miziolek, K.L. McNesby, R.A. Walters, Laser-induced breakdown spectroscopy (LIBS) — an emerging field-portable sensor technology for real-time, in-situ geochemical and environmental analysis, Geochemistry 5 (2005) 21–28.
[18] T. Hussain, M.A. Gondal, Z.H. Yamani, M.A. Baigkhak, Measurement of nutrients in green house soil with laser induced breakdown spectroscopy, Environ. Monit. Assess. 124 (2007) 131–139.
[19] F. Weritz, D. Schaurich, A. Taffe, G. Wilsch, Effect of heterogeneity on the quantitative determination of trace elements in concrete, Anal. Bioanal. Chem. 383 (2006) 248–255.
[20] M.E. Fraser, T. Panagiotou, A.J.R. Hunter, E.B. Anderson, S.J. Davis, Fugitive emission measurements above a hard Cr plating tank using spark induced breakdown spectroscopy, Plating Surface Finishing 87 (2000) 80–87.
[21] A.J.R. Hunter, S.J. Davis, L.G. Piper, K.W. Holtzclaw, M.E. Fraser, Spark-induced breakdown spectroscopy: a new technique for monitoring heavy metals, Appl. Spectrosc 54 (2000) 575–582.
[22] A.J.R. Hunter, J.R. Morency, C.L. Senior, S.J. Davis, M.E. Fraser, Continuous emission monitoring using spark induced breakdown spectroscopy, Appl. Optics 50 (2000) 111–117.
[23] D.A. Cremers, L.J. Radziemski, Handbook of Laser Induced Breakdown Spectroscopy, John Wiley & Sons, Chichester, 2006.
[24] A.W. Miziolek, V. Ralleschi, I. Schechtr, Laser-Induced Breakdown Spectroscopy, Cambridge University Press, 2006.
[25] B. Sallé, J.-L. Lacour, P. Mauchien, P. Fichet, S. Maurice, G. Manhès, Comparative study of different methodologies for quantitative rock analysis by laser-induced breakdown spectroscopy in a simulated Martian atmosphere, Spectrochimica Acta Part B 61 (2006) 301–313.